Towards first-principles prediction of valence instabilities in mixed stack charge-transfer crystals

Francesca Delchiaro, Alberto Girlando, and Anna Painelli*
Dipartimento di Chimica and INSTM-UdR Parma, Università di Parma, 43124 Parma, Italy

Arkamita Bandyopadhyay and Swapan K. Pati
New Chemistry Unit and Theoretical Sciences Unit, Jawaharlal Nehru Centre for Advanced Scientific Research, Bangalore-64, India

Gabriele D'Avino
Laboratory for the Chemistry of Novel Materials, University of Mons, Place du Parc 20, BE-7000 Mons, Belgium and Institut Néel, CNRS, 25 Rue des Martyrs, F-38042 Grenoble, France

(Received 30 December 2016; revised manuscript received 13 March 2017; published 17 April 2017)

Strongly correlated electrons delocalized on one-dimensional (1D) soft stacks govern the complex physics of mixed stack charge-transfer crystals, a well-known family of materials composed of electron-donor (D) and acceptor (A) molecules alternating along the 1D chain. The complex physics of these systems is well captured by a modified Hubbard model that also accounts for the coupling of electrons to molecular and lattice vibrational modes and for three-dimensional electrostatic interactions. Here we study several experimental systems to estimate relevant model parameters via density-functional theory calculations on DA units and isolated molecules and ions. Electrostatic intermolecular interactions, an important quantity not just to define the degree of charge transfer of the ground state but also to predict the propensity of the system towards multistability and hence towards discontinuous phase transitions, are also addressed. Results compare favorably with experimental data.

DOI: 10.1103/PhysRevB.95.155125

I. INTRODUCTION

Intermolecular charge-transfer (CT) interactions are responsible for the intriguing low-dimensional physics of CT crystals, an interesting family of compounds that include molecular conductors and superconductors and ferroelectric and multiferroic organic materials [1–4]. Among them, mixed stack CT (ms-CT) crystals are currently being intensively investigated as photoswitchable materials [5–9] as well as for ferroelectrics applications [3,10–12]. In ms-CT crystals π-electron donor (D) and acceptor (A) molecules alternate to form one-dimensional $\cdots$DADADA$\cdots$ stacks [13]. The sizable overlap between frontier orbitals along the stack leads to delocalized electrons in one dimension, and the D/A character of molecular units leads to alternating on-site charge $\cdots D^{\rho+}A^{\rho-}D^{\rho+}A^{\rho-}\cdots$. The specific value of ρ, the so-called degree of charge transfer or ionicity, depends on the relative electron-donating/accepting strength of the two molecules and on the intermolecular hopping t but is also affected by electrostatic intermolecular interactions, a concept that emerged very clearly with the discovery of the so-called neutral-ionic phase transition (NIT) [14,15]. NIT is an interesting phenomenon in which a ms-CT crystal with a formally neutral (N) state ($\rho < 0.5$) turns into a formally ionic (I) state ($\rho > 0.5$) upon decreasing temperature or increasing pressure as a result of the increase of the Madelung electrostatic energy following the lattice compression [16]. Quite interestingly, for systems close to a discontinuous NIT, a light pulse may also induce the transition, populating a long-lived metastable state [5–9].

As recognized in the early days of NIT, the N and I phases can be distinguished on a more fundamental basis than the ρ value [17–22]. Indeed, the nature of the ground state is qualitatively different in the two phases, with the I phase being unconditionally unstable with respect to dimerization, as confirmed by the dimerized stack structure observed for all known ionic ms-CT salts at low temperature. The very same existence of the Mott-insulating I phase points to the strongly correlated nature of ms-CT crystals and suggests describing the relevant physics based on a modified Hubbard model, accounting for on-site energy alternation $\pm\Delta$, the on-site Hubbard U, and the nearest-neighbor hopping integral t [17,19,23]. Indeed, current understanding of the physics of NIT is rooted in the strongly correlated physics described by Hubbard-like models.

Remarkable effects on vibrational spectra of ms-CT crystals were recognized early [24] and guided the extension of the model Hamiltonian to account for electron-vibration coupling [17,18,25,26]. Totally symmetric molecular vibrations of the D and A molecules modulate the energy of the relevant molecular orbital, while lattice modes modulate t. The resulting Hamiltonian then describes a fairly complex system, with correlated electrons delocalized along a one-dimensional (1D) soft lattice and responding to three-dimensional (3D) electrostatic interactions [27,28]. For a few systems, namely, TTF-CA [24] and the related DMTTF-CA [29], for which a large amount of experimental data are available, the model Hamiltonian has been parametrized and successfully exploited to describe and understand a large spectrum of experimental data [30,31].

Specifically, after an early assessment of vibronic coupling from the analysis of midinfrared (mid-IR) spectra [24], the model was parametrized against electronic absorption (CT) spectra [26]. The model was subsequently applied to describe diffuse x-ray signals [30], relating them to the softening of the dimerization mode in the proximity of the displacitive (anti)ferroelectric transition [32], a picture that was further

*anna.painelli@unipr.it

corroborated by a very detailed study of vibrational spectra in the far-IR region [33]. The calculation of the ground-state potential-energy surfaces of ms-CT crystals [28] set the basis to understand coexistence phenomena at the discontinuous phase transition but more generally pointed out the largely anharmonic nature of the phonons close to the phase transition. Accordingly, vibrational spectra were reinvestigated based on a dynamic treatment of vibrational motion that fully accounts for anharmonicity effects in infrared and Raman spectra of TTF-CA and DMTTF-CA [31]. An extension of the analysis to the excited state PES recently allowed us to describe, based on the same reference Hamiltonian, the vibrational dynamics following ultrafast excitation at NIT, fully disclosing subtle anharmonic effects due to the large coupling of molecular vibrations and lattice modes driven by their coupling to the electrons [34].

The model for TTF-CA and DMTTF-CA has therefore been quite extensively validated, and relevant model parameters are known with good confidence. A reliable parametrization of the model Hamiltonian for ms-CT crystals requires, however, a detailed analysis of a large set of experimental data, which is hardly available for most systems. Recently, an atomistic approach was proposed to extract the model parameters for ms-CT crystals based on first-principles calculations [35]. This strategy, successfully validated against TTF-CA, offers a useful tool to define reliable model parametrization for other ms-CT salts for which the lack of extensive experimental data hinders the application of the model Hamiltonian. In the present study this approach is applied to the parametrization of the modified Hubbard model for a large number of ms-CT salts with a regular stack structure, as listed in Fig. 1. Based on a mean-field description of electrostatic interactions and the adiabatic approximation for molecular vibrations, the first-principles parameters can be used to evaluate the ground-state ionicity of the crystal and, what is most interesting, to estimate the propensity of the material towards NIT and/or dimerization instabilities.

First-principles calculations, within the framework of periodic plane-wave density-functional theory (DFT), have also been applied to the description of the electronic structure of ms-CT crystals. These approaches proved successful in several respects, such as in reproducing the increase in the intermolecular CT (ionicity) in the transition from the high- to low-temperature structure of TTF-CA [36] or in describing the ferroelectric polarization of electronic origin of a few dimerized systems [4,37–39]. Here we follow a different approach that relies on ground-state DFT calculations for individual molecules and DA dimers and on the atomistic modeling of intermolecular electrostatic interactions to build a model for the crystal. Along these lines, we circumvent well-known pitfalls of local and semilocal density functionals in describing the physics of CT. Moreover, we explicitly account for the strong electronic correlations driving the NIT that are clearly missed in an effective single-particle picture such as DFT. Most interestingly, upon collapsing the complexity of several systems into a few physically meaningful parameters, our approach allows us to define reliable relationships between molecular properties, supramolecular organization in the solid state, and the electronic properties of the material. All this can then be rationalized within the framework of the universal

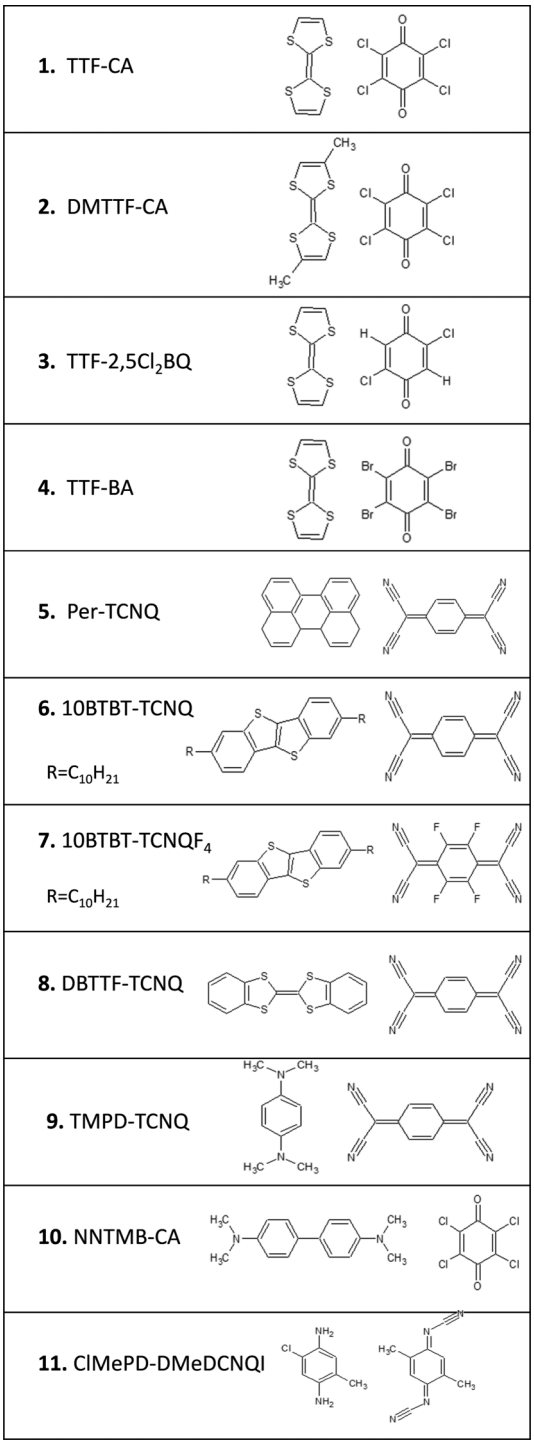

FIG. 1. Chemical structures of the systems of interest in this work. Chemical names associated with the abbreviations are as follows: DMTTF = 4,4′-dimethyltetrathiafulvalene; TTF = tetrathiafulvalene; CA = chloranil; $2,5Cl_2BQ$ = 2,5-dichloro-*p*-benzoquinone; BA = bromanil; Per = perylene; 10BTBT = 2,7-didecyl[1]benzothieno[3,2-*b*][1]benzothiophene; TCNQ = tetracyanoquinodimethane; $TCNQF_4$ = tetrafluoro-tetracyanoquinodimethane; DBTTF = dibenzotetrathiafulvalene; TMPD = *N*,*N*,*N*′,*N*′-tetramethyl-*p*-phenylenediamine; NNTMB = *N*,*N*,*N*′,*N*′-tetramethyl-benzidine; ClMePD = 2-chloro-5-methyl-*p*-phenylenediamine; DMeDCNQI = 2,5-dimethyl-dicyanoquinone-diimine.

picture of the N-I valence instability of ms-CT crystals provided by the modified Hubbard model accounting for electron-phonon coupling.

II. THE MODIFIED HUBBARD MODEL

Following previous work [28,31,34], we adopt the modified Hubbard model (MHM) to describe correlated electrons delocalized in one dimension along the mixed stack. In the strong-correlation limit we neglect states with double ionizations D^{2+} and A^{2-} achieving a large reduction of the dimension of the basis set [23]. With this approximation only two parameters define the Hubbard model, the hopping integral t and $\Gamma = \Delta - U/2$, the latter corresponding to half the energy required to transfer one electron from D to A molecules placed at infinite distance.

Electrostatic intermolecular interactions are important for NIT and enter the Hamiltonian with a set of parameters V_{ij} measuring the electrostatic interaction between two ionic molecules (either D^+ or A^-) located at i and j sites. We also account for the coupling with one effective molecular vibration Q, modulating the on-site energies, and with one effective lattice mode δ, modulating hopping integrals. For both vibrations we account for only the Brillouin-zone-center mode, which is relevant to optical spectroscopy and to the dimerization instability. The Hamiltonian reads

$$\begin{aligned} H_{rb} = {} & (\Gamma + Q)\sum_i (-1)^i \hat{n}_i \\ & - t\sum_{i,\sigma}[1 + (-1)^i\delta](\hat{a}^\dagger_{i,\sigma}\hat{a}_{i+1,\sigma} + \text{H.c.}) \\ & + \frac{1}{2}\sum_{i,j} V_{ij}\hat{\rho}_i\hat{\rho}_j + \frac{N}{2\epsilon_v}Q^2 + \frac{Nt^2}{2\epsilon_d}\delta^2, \end{aligned} \tag{1}$$

where i runs on the N sites of a stack, while the double sum i,j runs in three dimensions. Moreover, $\hat{a}_{i,\sigma}$ and $\hat{a}^\dagger_{i,\sigma}$ are the annihilation and creation operators for an electron with spin σ on site i, $\hat{n}_{i,\sigma} = \hat{a}^\dagger_{i,\sigma}\hat{a}_{i,\sigma}$ counts the electrons with spin σ on site i, $\hat{n}_i = \hat{n}_{i,\alpha} + \hat{n}_{i,\beta}$ counts the total number of electrons on the site, and the operators $\hat{\rho}_i = 2 - \hat{n}_i$ and $\hat{\rho}_i = \hat{n}_i$ measure the absolute value of the charge on D (odd i) and A (even i) sites, respectively. The vibrational relaxation energies, ϵ_v and ϵ_d, measure the lattice relaxation energy related to Q and δ modes, respectively. In the adiabatic approximation, we neglect vibrational kinetic energies.

In line with the adiabatic approximation, we define the equilibrium electronic Hamiltonian by substituting Q in the above equation with its equilibrium value, $Q_{\text{eq}} = \epsilon_v(1-\rho)$ [17], where ϵ_v is the intramolecular relaxation energy and $\rho = \langle\hat{\rho}_i\rangle$ is the average ionicity. Moreover, we adopt a mean-field (MF) approximation for electrostatic intermolecular interactions, reducing the problem of correlated electrons interacting in three dimensions into an effective 1D correlated-electron problem [40]. To such an aim, the 1D stack is seen as a collection of DA pairs. For each pair, $2z = 2\Gamma + V$ measures the energy required to transfer an electron from D to A accounting for the nearest-neighbor Coulomb interaction V. All other intermolecular electrostatic interactions in three dimensions are treated at the MF level, leading to the following Hamiltonian [17,28]:

$$\begin{aligned} H_{\text{eq}} = {} & z_{\text{eff}}\sum_i (-1)^i\hat{n}_i - t\sum_{i,\sigma}[1+(-1)^i\delta](\hat{a}^\dagger_{i,\sigma}\hat{a}_{i+1,\sigma}+\text{H.c.}) \\ & + \frac{N}{2}\epsilon_c\rho^2 - N\epsilon_c\rho + \frac{N}{2}\epsilon_v(1-\rho)^2 + \frac{Nt^2}{2\epsilon_d}\delta^2, \end{aligned} \tag{2}$$

where $z_{\text{eff}} = z - \epsilon_T\rho + \epsilon_v$ is half the energy required to ionize a DA pair accounting for the vibrational relaxation energy and for electrostatic intermolecular interactions and $\epsilon_T = \epsilon_c + \epsilon_v$. In turn, $\epsilon_c = V - 2M$ measures the strength of electrostatic interactions entering the MF, and $M = \frac{1}{2N}\sum_{ij} V_{ij}$ is the Madelung energy of a 3D lattice of fully ionic D and A molecules (notice that we adopt the standard convention with negative and positive signs for attractive and repulsive electrostatic interactions and we set the sign of ϵ_c as in Ref. [28] and opposite to Ref. [30]).

The MF Hamiltonian in Eq. (2) apparently contains only one-electron terms, although its representation on a real-space basis and its diagonalization account for its many-body nature. Indeed, correlated electrons are needed to describe the Mott-insulating I phase [41], and the adopted restricted basis approximation actually corresponds to the strong correlation limit ($U/t \to \infty$) of the Hubbard model in which doubly ionized states acquire infinite energy. The MF treatment of interstack electrostatic interactions is instrumental to collapse the 3D problem, which is untractable with many-body approaches, into an effective 1D correlated problem. The correlated Hamiltonian for a single stack can be diagonalized with an exact numerical treatment on finite-size systems, accounting explicitly for on-site Hubbard repulsion U and for electrostatic interactions within the stack. Results obtained along these lines for a model system with long-range Coulomb interactions demonstrate that the MF approximation works very well [18]. The MF treatment for all (inter- and intrastack) electrostatic interactions adopted here has the main advantage of collapsing all the needed information about the electrostatic interaction model into two parameters, V and ϵ_c, leading to a general description that allows us to rationalize the behavior of the whole family of ms-CT crystals without getting lost in a too detailed picture.

For fixed δ, the equilibrium Hamiltonian in Eq. (2) is defined by two parameters, z_{eff} and t, or better by a single parameter if t is set as the energy unit. Solving the problem for different z_{eff} values yields a universal $\rho(z_{\text{eff}}/t)$ curve that was first obtained for systems with up to 12 sites in Ref. [17] for $\delta = 0$. Here we extend the results to 16-site chains. The results, reported in Fig. S3 in the Supplemental Material [42], show smooth $\rho(z_{\text{eff}}/t)$ evolution for $N = 4n + 2$ systems, while, due to a well-known symmetry crossover [17,27], $N = 4n$ systems show an ionicity jump whose amplitude decreases quickly with increasing system size. A continuous curve can be extrapolated in the infinite-chain limit [17] in a procedure that is facilitated by the observation that the $N = 4n$ and $N = 4n + 2$ results converge to the same limit from opposite directions, making extrapolation uncertainties no larger than 5% in the critical region (see Fig. S3).

From the universal $\rho(z_{\text{eff}}/t)$ curve it is possible to extract, for fixed $\epsilon_T = \epsilon_c + \epsilon_v$ values, the relevant $z = z_{\text{eff}} + \epsilon_T\rho - \epsilon_v$ and finally get the z dependence of electronic properties. The

$\rho(z)$ curve becomes steeper and steeper with increasing ϵ_T, and for ϵ_T larger than a critical value estimated as $1.8t$ it becomes S-shaped, with a region of positive slope corresponding to unstable states. In other terms, electrostatic intermolecular interactions and the on-site vibrational coupling cooperate towards bistability in ms-CT crystals, making states of intermediate ionicity unattainable and opening a bistability window where both quasineutral and quasi-ionic states are accessible.

III. MHM PARAMETERS FROM FIRST-PRINCIPLES CALCULATIONS

We now discuss how the microscopic parameters of the MHM can be extracted from first-principles methods, with the notable exception of ϵ_d, which is not relevant to the present analysis focusing on only regular (nondimerized) $\cdots$DADADA$\cdots$ stacks. To be specific and to illustrate the power and simplicity of our approach, we will discuss results obtained for several crystals, as listed in Fig. 1. These crystals have been selected as representative examples of systems made up of chemically different D and A species, well characterized in terms of crystal structure and with a known ionicity appreciably different from zero.

Following the approach in Ref. [35], the two parameters defining the electronic problem, z and t, can be obtained by mapping the singlet and triplet states of the MHM relevant to a DA pair into the lowest singlet and triplet states obtained from DFT calculations on a DA pair in the crystallographic geometry. Specifically, the basis states for the MHM of a DA pair in the reduced basis are two singlet states describing the neutral and ionic pair, $|\mathrm{DA}\rangle_S$ and $|\mathrm{D}^+\mathrm{A}^-\rangle_S$, respectively, and the triplet ionic states $|\mathrm{D}^+\mathrm{A}^-\rangle_T$. The triplet states stay unmixed, while the two singlet states, separated by an energy gap $2z$ and mixed by a matrix element $\sqrt{2}t$, combine into a ground state $\Psi_G = \sqrt{1-\rho_{\mathrm{dim}}}|\mathrm{DA}\rangle_S + \sqrt{\rho_{\mathrm{dim}}}|\mathrm{D}^+\mathrm{A}^-\rangle_S$, where

$$\rho_{\mathrm{dim}} = \frac{1}{2}\left(1 - \frac{z/t}{\sqrt{(z/t)^2+2}}\right) \tag{3}$$

measures the amount of charge transfer in the isolated DA pair and depends only on the z/t ratio. We stress that ρ_{dim} is not related to the ionicity ρ relevant to the crystal, which is also affected by 3D electrostatic interactions. The triplet-singlet energy gap

$$\Delta_{ST} = z + t\sqrt{(z/t)^2+2} \tag{4}$$

gives an independent expression, so that a DFT estimate of ρ_{dim} and Δ_{ST} allows for the estimate of parameters z and t.

DFT calculations (GAUSSIAN09 package [43]) are performed on DA pairs relevant to the different crystals considered in this work, as detailed in the Supplemental Material [42]. For most salts the choice of the DA pair is unambiguous since the crystal can be constructed as the repetition of a single DA pair. TTF-BA represents a notable exception, being characterized by two mutually orthogonal and nonequivalent stacks [44]. In this case, two different TTF-BA pairs, indicated with suffixes (a) and (b) in Table I, are extracted from the crystal structure. In the disordered ClMePD-DMeDCNQI crystal [45] the chlorine atom and the methyl group have 1:1 occupancy at each site, originating two inequivalent pairs, again indicated by suffixes (a) and (b). In either case the typical C-Cl distance (1.71 Å) is used. When the position of H atoms is not explicitly given in the crystallographic structure, they are added optimizing their position based on semiempirical calculations according to the PM7 parametrization as defined in MOPAC package [46]. All calculations are performed in vacuum using the ωB97XD hybrid functional, as defined in GAUSSIAN09 package [43] that, adopting a range-separated treatment of the Coulomb operator and including dispersion corrections, is particularly well suited for modeling intermolecular CT [47]. The basis set 6-31+G* [43] has been chosen to include both anisotropic distribution and electron distribution far away from the nuclei (important for lone-pair systems and anions). As discussed in Refs. [35,48] and explicitly verified for some systems, the choice of the functional is not crucial, marginally affecting calculated quantities.

TABLE I. DFT triplet-singlet energy difference (eV) and singlet and triplet ionicities for DA pairs at the geometry of the crystallographic structure.

System	$E_T - E_{\mathrm{gs}}$	ρ_{dim}	ρ^T_{dim}
1. TTF-CA [49]	0.988	0.091	0.867
2. DMTTF-CA [50]	0.887	0.097	0.864
3. TTF-2,5Cl_2BQ [51]	1.205	0.097	0.792
4. TTF-BA(a) [44]	0.273	0.121	0.946
4. TTF-BA(b) [44]	0.419	0.128	0.947
5. Per-TCNQ [52]	1.171	0.109	0.867
6. 10BTBT-TCNQ [53]	1.595	0.046	0.736
7. 10BTBT-TCNQF_4 [53]	1.218	0.064	0.880
8. DBTTF-TCNQ [54]	0.739	0.155	0.860
9. TMPD-TCNQ [55]	−0.350	0.244	0.813
10. NNTMB-CA [56]	1.883	0.070	0.841
11. ClMePD-DMeDCNQI(a) [45]	1.096	0.178	0.871
11. ClMePD-DMeDCNQI(b) [45]	1.034	0.188	0.882

Table I reports for each DA pair the difference between the ground-state triplet and singlet energies E_T and E_{gs} as well as the relevant charges, ρ_{dim} and ρ^T_{dim}, estimated from the Hirshfeld charges. The charge for the triplet state ρ^T_{dim} does not enter the estimate of z and t but is shown for a consistency check: in the MHM the triplet state is a pure charge-separated state, so that we would expect $\rho^T_{\mathrm{dim}} = 1$. The relatively modest deviations of the calculated ρ^T_{dim} from this limiting value give confidence to the quality of the proposed approach.

TMPD-TCNQ shows an anomalous behavior, with the triplet state lying lower in energy than the singlet one. This anomaly is plausibly ascribed to the variation of geometry of the TMPD molecule upon ionization: the neutral molecule has a pyramidal structure of the N-terminal groups that becomes planar in the quinoidal TMPD^+ radical ion. TMPD-TCNQ has a largely ionic ground state [57], with approximately planar TMPD molecules in the x-ray crystal structure [55]. In the dimer calculations the electrostatic interactions are not sufficient to drive the system to an ionic state (the ionicity calculated for the dimer in the lowest singlet state is 0.244), but the neutral state is destabilized by the frustrated molecular geometry, leading to singlet-triplet inversion. A triplet ground

TABLE II. Estimated model parameters for the MHM. All parameters have eV energy units.

System	z	t	ϵ_v	V	M	ϵ_c
1. TTF-CA	0.44	0.22	0.47	− 2.53	− 1.65	0.77
2. DMTTF-CA	0.40	0.21	0.49	− 2.41	− 1.20	− 0.02
3. TTF-2,5,Cl_2BQ	0.54	0.28	0.49	− 2.58	− 1.31	0.54
4. TTF-BA(a)	0.12	0.07	0.45	− 2.36	− 1.46	0.56
4. TTF-BA(b)	0.18	0.11	0.45	− 2.62	− 1.46	0.29
5. Per-TCNQ	0.51	0.29	0.31	− 2.05	− 1.03	0.01
6. 10BTBT-TCNQ	0.76	0.25	0.36	− 2.00	− 1.00	0.00
7. 10BTBT-TCNQF_4	0.57	0.23	0.36	− 1.89	− 0.95	0.02
8. DBTTF-TCNQ	0.30	0.22	0.36	− 2.01	− 1.04	0.07
10. NNTMB-CA	0.87	0.37	0.58	− 2.26	− 1.01	− 0.24
11. ClMePD-DMeDCNQI(a)	0.43	0.36	0.82	− 2.43	− 1.21	0.02
11. ClMePD-DMeDCNQI(b)	0.40	0.35	0.82	− 2.41	− 1.21	− 0.01

state is definitely not consistent with the MHM model for the dimer and does not allow for the mapping. Accordingly, we will not discuss this system in the following. For all other systems, data in Table I allow us to extract the z and t values as listed in Table II.

It is well known that the energy required to ionize a DA complex is largely affected by a polarizable environment. Indeed, the dipole field generated by a D^+A^- pair polarizes the environment, and this induced polarization in turn stabilizes the CT configuration. The MHM model fully accounts for the intermolecular CT polarizability but neglects the internal structure of the molecules and hence their intrinsic polarizability. On the other hand, DFT calculations in the vacuum miss the important contribution from the polarizability of the surrounding molecules. We account for this contribution through the renormalization $2z \rightarrow 2z^* = 2(z + \Gamma_P)$, where $\Gamma_P < 0$ accounts for the polarizable environment [35].

To estimate Γ_P we adopt the intramolecular charge redistribution model, describing the molecular anisotropic polarization in terms of charge flows among atoms and induced dipoles [58]. Specifically, we evaluate the extensive electrostatic energy of the N crystal U_N and the energy of a N crystal with a single ionized DA pair $U_{D^+A^-}$ in a special location and finally calculate $2\Gamma_P = U(D^+A^-) - U(N)$. In practice, calculations are performed on finite spherical clusters centered around the special location, and $2\Gamma_P$ is obtained by extrapolating to the infinite-radius limit [35]. Charge-redistribution calculations have been performed with the MESCAL code [59].

For TTF-CA the value $\Gamma_P = -0.19$ eV was obtained previously [35]. Here we explicitly estimate $\Gamma_P = -0.23$ eV for TTF-BA and $\Gamma_P = -0.20$ eV for ClMePD-DMeDCNQI. Since all calculated corrections are very similar, with variations well within the uncertainties of other estimated quantities, we apply the same correction of -0.2 eV to all systems defining $z^* = (z + \Gamma_P)$ that will be used in the following MHM calculations.

Three additional parameters are needed to fully describe ms-CT salts with a regular stack. The first one, ϵ_v, the vibrational relaxation energy, measures the stabilization of the ionic $|D^+A^-\rangle$ state due to the vibrational relaxation of the D and A sites upon ionization. This quantity can be easily estimated as the sum of the relaxation energies calculated for the isolated D and A species. Specifically, DFT calculations of isolated (gas-phase) neutral D and A molecules are used to obtain the equilibrium geometry for the neutral species. The relaxation energy is then calculated as the difference between the energy of the ionic D^+ and A^- species calculated for the same geometry as obtained for the neutral species and in the relaxed geometry. Results are shown in Table II.

Finally, electrostatic interaction energies, V and M (from which we derive $\epsilon_c = V - 2M$) in Table II, are obtained resorting to a point-charge approximation of the molecular charge density [35]. We resort to electrostatic potential (ESP) atomic charges derived from the fitting of the molecular electrostatic potential [60] that we specifically compute for neutral and charged molecules. Our approach approximates intermolecular interactions as the sum of pairwise unscreened electrostatic interactions between point charges located at atomic positions. The dielectric screening provided by molecular polarizabilities, as estimated with the intramolecular charge redistribution model [58,59], has been shown to provide only a minor correction to the value of V and M in TTF-CA and other ms-CT crystals [35]. The nearest-neighbor (intrapair) interaction energy between ionic species is defined as $V = V_I - V_N$, where V_I and V_N are the intermolecular electrostatic interactions between radical ions (D^+ and A^-) and neutral molecules (D and A), respectively. Finally, the Madelung energy M, entering the expression for ϵ_c, is again obtained as the difference between the total electrostatic energy for a lattice of ionic D^+ and A^- sites and the same quantity evaluated for a lattice of neutral D and A sites. Explicit results for V_I, V_N, M_I, and M_N are reported in the Supplemental Material [42].

By looking at Table II, we observe that t shows a fairly large variability, ranging from a very low value <0.1 eV for TTF-BA up to 0.36 eV for NNTMB-CA. Variations of V are far less important, ranging from -1.9 eV (10BTBT − $TCNQF_4$) to -2.6 [TTF-BA(b)]. The comparable magnitude of V values follows from the similar molecular dimensions and intermolecular nearest-neighbor distance in mixed stacks. Negative V values point to attractive intramolecular electrostatic interactions, as expected on physical grounds for ions of opposite polarity (D^+A^-). More interesting is the ϵ_c variation. The Madelung energy for an ionic DA stack is clearly negative (attractive intermolecular interactions are expected): negative ϵ_c values in Table II point to the presence of dominant repulsive

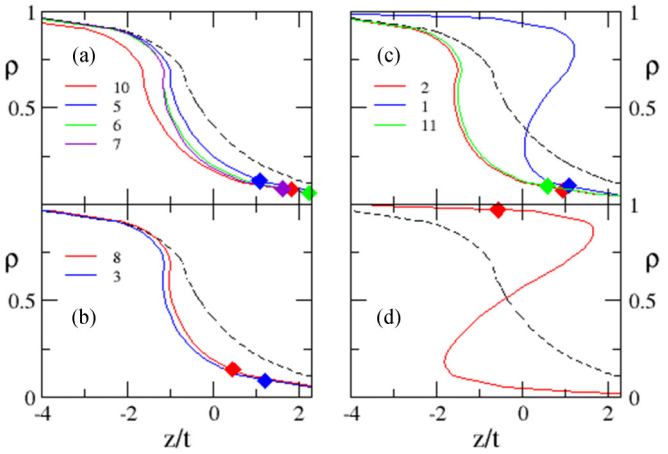

FIG. 2. Results of MHM calculations for ten CT crystals defined in Fig. 1. The different panels group the crystals according to the ϵ_T/t values: (a) $\epsilon_T < 1.8t$, all values of ρ are accessible; (b) $\epsilon_T \sim 1.8t$ marginally bistable systems; (c) $\epsilon_T > 1.8t$ bistable systems; and (d) $\epsilon_T \gg 1.8t$ extreme bistability. In all panels the dashed black line is the universal $\rho(z/t)$ curve; colored lines refer to the specific systems numbered as in Fig. 1 and obtained with the parameters in Table II. Diamonds show the ionicity computed for the z/t value obtained from the atomistic parametrization.

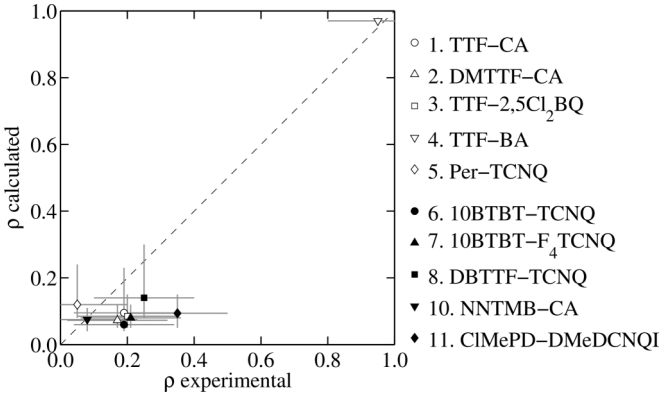

FIG. 3. Experimental ρ values vs calculated results for ten CT crystals defined in Fig. 1. A generally good agreement is found between experiment and theory, with most points falling on the ideal 1:1 (dashed) line within the uncertainties of calculations and experiments (error bars). Experimental ionicities are taken from Ref. [61] for TTF-CA, [29] for DMTTF-CA, [51] for TTF-2,5Cl_2BQ, [62] for TTF-BA, [63] for Per-TCNQ, [53] for 10BTBT-TCNQ and 10BTBT-F_4TCNQ, [64] for DBTTF-TCNQ, [65] for NNTMB-CA, and [66] for ClMePD-DMeDCNQI.

interstack interactions, overwhelming the attractive intrastack interactions. Indeed, systems with negative ϵ_c typically have D-D and/or A-A dominant interstack interactions.

IV. GROUND-STATE PROPERTIES OF MS-CT CRYSTALS FROM DFT

We are now in the position to analyze the ground-state properties of several systems discussed in this work based on the model described in Sec. II and on the DFT-based parametrization in Sec. III. The universal $\rho(z_{\rm eff}/t)$ obtained from the extrapolation of finite-size results (see Fig. S3) is shown as a dashed black line in all panels of Fig. 2. From this curve we can extract the $\rho(z/t)$ curve specific for each investigated system using the ϵ_v/t and $\epsilon_T/t = (\epsilon_c + \epsilon_v)/t$ listed in Table III. For TTF-BA and ClMePD-DMeDCNQI, for which two inequivalent pairs were discussed, we just report averaged results. Finally, the estimated z^*/t values in Table III fix the relevant abscissa point for each system at hand, thus allowing us to extract a theoretical estimate for ρ, shown as diamonds in Fig. 2.

TABLE III. Estimated model parameters entering the mean-field description of the MHM.

System	ϵ_T/t	ϵ_v/t	z^*/t
1. TTF-CA	5.63	2.13	1.11
2. DMTTF-CA	2.29	2.38	0.95
3. TTF-2,5Cl_2BQ	1.93	1.76	1.21
4. TTF-BA	9.46	4.86	−0.56
5. Per-TCNQ	1.12	1.07	1.08
6. 10BTBT-TCNQ	1.45	1.45	2.25
7. 10BTBT-TCNQF_4	1.67	1.60	1.63
8. DBTTF-TCNQ	1.91	1.61	0.46
10. NNTMB-CA	0.94	1.59	1.84
11. ClMePD-DMeDCNQI	2.31	2.30	0.59

A direct comparison between the calculated and experimental values of ρ for all the systems considered in this study is provided in Fig. 3. Experimental results report the best estimate of room-temperature ionicity for the crystals (see references in the figure caption). To make the comparison meaningful we set an error bar of the order of 0.15 on experimental estimates of ρ. The uncertainty on the calculated ρ values can be easily estimated for each system from the curves in Fig. 2, provided an estimate of the uncertainty of z/t is given. We set the z/t uncertainty to $\sim$1 on the basis of Eq. (3), under the assumption of an uncertainty on the calculated $\rho_{\rm dim}$ of the order of 0.1. Results in Fig. 3 suggest that the described approach gives reliable estimates of the ionicity, even if a general tendency to underestimate the ionicity is observed.

We notice that microscopic parameters are extracted from room-temperature crystallographic structures, with the notable exception of perylene-TCNQ, whose crystal structure data are collected at 150 K. However, properties of perylene-TCNQ are marginally affected by temperature. We also notice that we address only ground-state (zero-temperature) properties of the MHM; however, charge degrees of freedom are located for ms-CT salts at energies well above thermal energies at room temperature, so we do not expect any variation in the calculated ρ if finite temperature is accounted for.

The prediction of the ionicity of ms-CT crystals is not the most important result of this work. Indeed, the curves in Fig. 2 offer a valuable insight into the valence instability region of the considered CT crystals. Four systems, Per-TCNQ, 10BTBT-TCNQ, 10BTBT-TCNQF_4, and NNTMB-CA [Fig. 2(a)], have $\epsilon_T/t < 1.8$, and the relevant curves do not show any sign of bistability. Two systems, TTF-2,5,Cl_2BQ and DBTTF-TCNQ [Fig. 2(b)], with $\epsilon_T/t \sim 1.9$, are marginally bistable. The remaining four systems (DMTTF-CA, ClMePD-DMeDCNQI,

TTF-CA, and TTF-BA) show bistability with an increasingly sizable unaccessible region of intermediate ρ values.

We are now in the position of verifying the prediction of our model with the experimental behavior of the considered systems with respect to the valence instability. Per-TCNQ, 10BTBT-TCNQ, 10BTBT-TCNQF$_4$, and NNTMB-CA have small ionicities at room temperature as a consequence of the large energy gap $2z$ (Table II) and no predicted valence instabilities. For TTF-CA [Fig. 2(c)] we predict that ionicities in the range from approximately 0.3 to 0.8 are not accessible, and indeed, at room temperature TTF-CA shows a regular stack structure with $\rho \sim 0.2$. Upon decreasing the temperature the ionicity of TTF-CA increases up to 0.3, and then when reaching 81 K, a discontinuous NIT occurs, driving the system in the ionic regime with $\rho \sim 0.52$ and a dimerized stack structure (by further lowering the temperature, ρ increases up to 0.6 at 10 K) [67]. DMTTF-CA shows a much smaller instability region: according to Fig. 2(c), it is stable up to $\rho \sim 0.5$. For ionicities larger than ≈ 0.3 one expects instability towards dimerization [18], and indeed, at 65 K DMTTF-CA undergoes a dimerization transition, while ρ increases continuously or almost so from ~ 0.2 at room temperature to ~ 0.4 at10K [29]. The cases of TTF-2,5Cl$_2$BQ and DBTTF-TCNQ are of particular significance when compared with the above-discussed TTF-CA and DMTTF-CA. The room-temperature ionicity of these four crystals (between 0.2 and 0.3) is, in fact, very similar to that of TTF-CA, yet TTF-2,5Cl$_2$ and DBTTF-TCNQ do not undergo any charge instability down to 10 K. This is in line with the lower value of ϵ_T/t calculated for these systems (Table II). ClMePD-DMeDCNQI [Fig. 2(c)] has an ϵ_T/t slightly larger than that of DMTTF-CA, but the actual system is affected by disorder, which prevents long-range ordering: ClMePD-DMeDCNQI presents a parallel increase of dimerization and ionicity, being the only example of a continuous ionicity change from quasineutral at room temperature ($\rho \approx 0.35$) to quasi-ionic ($\rho \approx 0.6$) at 80 K [45]. Finally, for TTF-BA in Fig. 2(d) we predict an enormous instability region, which can be ascribed to the very small t value and to the corresponding very large ϵ_T/t values. According to Fig. 2(d), TTF-BA can be only largely neutral, with $\rho < 0.15$, or largely ionic, with $\rho > 0.9$; all intermediate ionicity values are forbidden. The estimated value of z^*/t places the crystal on the ionic side, and indeed, experimentally TTF-BA is largely ionic, with $\rho > 0.95$, and undergoes a dimerization transition upon decreasing temperature [62].

V. CONCLUSIONS

An extensive set of DFT calculations for isolated DA dimers extracted from the crystallographic data available for several ms-CT crystals on corresponding D and A molecules and ions in the gas phase has been used to estimate basic model parameters entering the modified Hubbard model. The atomic charges obtained from DFT are used to estimate electrostatic interactions between fully charged species, V and ϵ_c, as needed to describe the ground-state properties of mixed stack CT salts in the mean-field approximation. This systematic work validates on several different systems an approach recently proposed by D'Avino and Verstraete [35], demonstrating its wide applicability: indeed, only 1 out of 11 studied systems could not be parametrized following the proposed approach.

The analysis of several crystals, showing a very different (and well-studied) behavior, demonstrates that this simple and computationally inexpensive method can be used to predict, based on the crystallographic structure, the ground-state ionicity and, in general, the ground-state properties of ms-CT crystals. More interestingly, the proposed approach, integrated with the MF treatment of electrostatic intermolecular interactions and the adiabatic treatment of the on-site electron-vibration coupling, allows one to derive a satisfactory description of the charge instabilities of the system at hand.

Hubbard-like models offers a comparatively simple description of strongly correlated electrons: accounting for a minimal set of frontier orbitals and electrons, they can be diagonalized exactly in some cases, or at least they are amenable to a numerically exact solution for large enough systems to get reliable information about the thermodynamic limit. Moreover, only a limited number of essential interactions are introduced in the model, allowing us to maintain the main physics of the system under control. The major drawback of the Hubbard-like Hamiltonian is its semiempirical nature: model parameters must be guessed and validated against experiment. First-principles models, including DFT approaches, are nominally free from adjustable parameters (the functionals are, indeed, usually parametrized, even if not on the specific system at hand) but, accounting for all electrons and a large orbital basis, are not amenable to exact solutions. Strongly correlated electrons are poorly described in DFT. The proposed approach combines the best features of the two worlds: the simplicity of the MHM is maintained while model parameters are extracted from DFT calculations run on very small molecular clusters (actually dimers), according to a mapping strategy similar to the one proposed many years back for bis(ethylenedithio)tetrathiafulvalene (BEDT-TTF) superconductors [68]. Electrostatic intermolecular interactions play a major in ms-CT crystals and can be evaluated from crystal structure data once the charge distribution is calculated for the isolated D and A molecules and relevant ions (D^+ and A^-). Reliable estimates of the electron-molecular vibration coupling are also obtained from DFT calculation on the isolated molecules and ions.

Exploiting valence bond calculations, ground-state properties of a general MHM Hamiltonian can be obtained for very large chains, fully accounting for correlated electrons delocalized in a 1D stack. A mean-field treatment of interstack interactions that maintains the strongly correlated nature of the system and an adiabatic description of electron-molecular vibration coupling lead to a very general and powerful description of the charge instability of mixed stack CT crystals, allowing us to rationalize the behavior of a large family of systems.

ACKNOWLEDGMENTS

Work in Parma was supported by the Italian Ministry of Research and Education (MIUR) through Grant No. PRIN-2012T9XHH7 and by CINECA through Grant No. ISCRAC-HP10CAUAMP. The India-Italy cooperation was

supported by the Italian Ministry of Foreign Affairs and by the Indian Department of Science and Technology through the Indo-Italian executive program. G.D. thanks M. J. Verstraete for fruitful discussions and acknowledges support from the EU through the FP7-PEOPLE-2013-IEF program (Project no. 625198).

[1] G. Saito and Y. Yoshida, Bull. Chem. Soc. Jpn. **80**, 1 (2007).
[2] S. Tomic and M. Dressel, Rep. Prog. Phys. **78**, 096501 (2015).
[3] S. Horiuchi and Y. Tokura, Nat. Mater. **7**, 357 (2008).
[4] G. Giovannetti, S. Kumar, A. Stroppa, J. van den Brink, and S. Picozzi, Phys. Rev. Lett. **103**, 266401 (2009).
[5] T. Suzuki, T. Sakamaki, K. Tanimura, S. Koshihara, and Y. Tokura, Phys. Rev. B **60**, 6191 (1999).
[6] T. Luty, H. Cailleau, S. Koshihara, E. Collet, M. Takesada, M. H. Lemée-Cailleau, M. B.-L. Cointe, N. Nagaosa, Y. Tokura, E. Zienkiewicz, and B. Ouladdiaf, Europhys. Lett. **59**, 619 (2002).
[7] E. Collet, M.-H. Lemée-Cailleau, M. B.-L. Cointe, H. Cailleau, M. Wulff, T. Luty, S.-Y. Koshihara, M. Meyer, L. Toupet, P. Rabiller, and S. Techert, Science **300**, 612 (2003).
[8] H. Okamoto, Y. Ishige, S. Tanaka, H. Kishida, S. Iwai, and Y. Tokura, Phys. Rev. B **70**, 165202 (2004).
[9] S. Iwai, Y. Ishige, S. Tanaka, Y. Okimoto, Y. Tokura, and H. Okamoto, Phys. Rev. Lett. **96**, 057403 (2006).
[10] F. Kagawa, S. Horiuchi, H. Matsui, R. Kumai, Y. Onose, T. Hasegawa, and Y. Tokura, Phys. Rev. Lett. **104**, 227602 (2010).
[11] F. Kagawa, S. Horiuchi, M. Tokunaga, J. Fujioka, and Y. Tokura, Nat. Phys. **6**, 169 (2010).
[12] K. Kobayashi, S. Horiuchi, R. Kumai, F. Kagawa, Y. Murakami, and Y. Tokura, Phys. Rev. Lett. **108**, 237601 (2012).
[13] Z. G. Soos and D. J. Klein, in *Treatise on Solid-State Chemistry*, edited by N. B. Hannay (Plenum Press, New York, 1976), Vol. 3, p. 679.
[14] J. B. Torrance, J. E. Vazquez, J. J. Mayerle, and V. Y. Lee, Phys. Rev. Lett. **46**, 253 (1981).
[15] J. B. Torrance, A. Girlando, J. J. Mayerle, J. I. Crowley, V. Y. Lee, P. Batail, and S. J. LaPlaca, Phys. Rev. Lett. **47**, 1747 (1981).
[16] A. Girlando, A. Painelli, S. A. Bewick, and Z. G. Soos, Synth. Met. **141**, 129 (2004), and references therein.
[17] A. Girlando and A. Painelli, Phys. Rev. B **34**, 2131 (1986).
[18] A. Painelli and A. Girlando, Phys. Rev. B **37**, 5748 (1988).
[19] N. Nagaosa and J.-I. Takimoto, J. Phys. Soc. Jpn. **55**, 2735 (1986).
[20] N. Nagaosa and J.-I. Takimoto, J. Phys. Soc. Jpn. **55**, 2745 (1986).
[21] N. Nagaosa, J. Phys. Soc. Jpn. **55**, 2754 (1986).
[22] M. Avignon, C. A. Balseiro, C. R. Proetto, and B. Alascio, Phys. Rev. B **33**, 205 (1986).
[23] Z. G. Soos, R. H. Harding, and S. Ramasesha, Mol. Cryst. Liq. Cryst. **125**, 59 (1985).
[24] A. Girlando, F. Marzola, C. Pecile, and J. B. Torrance, J. Chem. Phys. **79**, 1075 (1983).
[25] A. Painelli and A. Girlando, J. Chem. Phys. **84**, 5655 (1986).
[26] A. Painelli and A. Girlando, J. Chem. Phys. **87**, 1705 (1987).
[27] Y. Anusooya-Pati, Z. G. Soos, and A. Painelli, Phys. Rev. B **63**, 205118 (2001).
[28] Z. G. Soos and A. Painelli, Phys. Rev. B **75**, 155119 (2007).
[29] P. Ranzieri, M. Masino, A. Girlando, and M.-H. Lemée-Cailleau, Phys. Rev. B **76**, 134115 (2007).
[30] G. D'Avino, A. Girlando, A. Painelli, M.-H. Lemée-Cailleau, and Z. G. Soos, Phys. Rev. Lett. **99**, 156407 (2007).
[31] G. D'Avino, M. Masino, A. Girlando, and A. Painelli, Phys. Rev. B **83**, 161105 (2011).
[32] L. DelFreo, A. Painelli, and Z. G. Soos, Phys. Rev. Lett. **89**, 027402 (2002).
[33] A. Girlando, M. Masino, A. Painelli, N. Drichko, M. Dressel, A. Brillante, R. G. D. Valle, and E. Venuti, Phys. Rev. B **78**, 045103 (2008).
[34] L. Cavatorta, A. Painelli, and Z. G. Soos, Phys. Rev. B **91**, 174301 (2015).
[35] G. D'Avino and M. J. Verstraete, Phys. Rev. Lett. **113**, 237602 (2014).
[36] P. Garcia, S. Dahaoui, C. Katan, M. Souhassou, and C. Lecomte, Faraday Discuss. **135**, 217 (2007).
[37] S. Ishibashi and K. Terakura, Phys. B (Amsterdam, Neth.) **405**, S338 (2010).
[38] S. Ishibashi, K. Terakura, and S. Horiuchi, J. Phys. Soc. Jpn. **79**, 043703 (2010).
[39] S. Ishibashi, S. Horiuchi, R. Kumai, and K. Terakura, Phys. Status Solidi B **249**, 1008 (2012).
[40] Z. G. Soos and S. Mazumdar, Phys. Rev. B **18**, 1991 (1978).
[41] A. Painelli and A. Girlando, Phys. Rev. B **45**, 8913 (1992).
[42] See Supplemental Material at http://link.aps.org/supplemental/10.1103/PhysRevB.95.155125 for the crystallographic information of the studied compounds and for the calculation of the electrostatic interactions.
[43] M. J. Frisch, G. W. Trucks, H. B. Schlegel, G. E. Scuseria, M. A. Robb, J. R. Cheeseman, G. Scalmani, V. Barone, B. Mennucci, G. A. Petersson, H. Nakatsuji, M. Caricato, X. Li, H. P. Hratchian, A. F. Izmaylov, J. Bloino, G. Zheng, J. L. Sonnenberg, M. Hada, M. Ehara, K. Toyota, R. Fukuda, J. Hasegawa, M. Ishida, T. Nakajima, Y. Honda, O. Kitao, H. Nakai, T. Vreven, J. A. Montgomery, Jr., J. E. Peralta, F. Ogliaro, M. Bearpark, J. J. Heyd, E. Brothers, K. N. Kudin, V. N. Staroverov, R. Kobayashi, J. Normand, K. Raghavachari, A. Rendell, J. C. Burant, S. S. Iyengar, J. Tomasi, M. Cossi, N. Rega, J. M. Millam, M. Klene, J. E. Knox, J. B. Cross, V. Bakken, C. Adamo, J. Jaramillo, R. Gomperts, R. E. Stratmann, O. Yazyev, A. J. Austin, R. Cammi, C. Pomelli, J. W. Ochterski, R. L. Martin, K. Morokuma, V. G. Zakrzewski, G. A. Voth, P. Salvador, J. J. Dannenberg, S. Dapprich, A. D. Daniels, Farkas, J. B. Foresman, J. V. Ortiz, J. Cioslowski, and D. J. Fox, GAUSSIAN09 revision E.01 (Gaussian Inc., Wallingford, CT, 2009).
[44] P. García, S. Dahaoui, P. Fertey, E. Wenger, and C. Lecomte, Phys. Rev. B **72**, 104115 (2005).
[45] S. A. Bewick, R. A. Pascal, D. M. Ho, Z. G. Soos, M. Masino, and A. Girlando, J. Chem. Phys. **122**, 024710 (2005).
[46] J. J. P. Stewart, J. Mol. Model. **19**, 1 (2013).

[47] J.-D. Chai and M. Head-Gordon, Phys. Chem. Chem. Phys. **10**, 6615 (2008).
[48] A. Bandyopadhyay and S. K. Pati, Chem. Phys. Lett. **624**, 64 (2015).
[49] J. J. Mayerle, J. B. Torrance, and J. I. Crowley, Acta Crystallogr., Sect. B **35**, 2988 (1979).
[50] S. Horiuchi, Y. Okimoto, R. Kumai, and Y. Tokura, Science **299**, 229 (2003).
[51] A. Girlando, A. Painelli, C. Pecile, G. Calestani, C. Rizzoli, and R. M. Metzger, J. Chem. Phys. **98**, 7692 (1993).
[52] I. J. Tickle and C. K. Prout, J. Chem. Soc., Perkin Trans. 2, 727 (1973).
[53] H. Mendez, G. Heimel, A. Opitz, K. Sauer, P. Barkowski, M. Oehzelt, J. Soeda, T. Okamoto, J. Takeya, J. B. Arlin, J. Y. Balandier, Y. Geerts, N. Koch, and I. Salzmann, Angew. Chem., Int. Ed. **52**, 7751 (2013).
[54] T. J. Emge, F. M. Wiygul, J. S. Chappell, A. N. Bloch, J. P. Ferraris, D. O. Cowan, and T. J. Kistenmacher, Mol. Cryst. Liq. Cryst. **87**, 137 (1982).
[55] A. W. Hanson, Acta Cryst. **19**, 610 (1965).
[56] K. Yakushi, I. Ikemoto, and H. Kuroda, Acta Crystallogr., Sect. B **29**, 2640 (1973).
[57] A. Girlando, A. Painelli, and C. Pecile, Mol. Cryst. Liq. Cryst. **112**, 325 (1984).
[58] E. V. Tsiper and Z. G. Soos, Phys. Rev. B **64**, 195124 (2001).
[59] G. D'Avino, L. Muccioli, C. Zannoni, D. Beljonne, and Z. G. Soos, J. Chem. Theory Comput. **10**, 4959 (2014).
[60] B. H. Besler, K. M. Merz, and P. A. Kollman, J. Comput. Chem. **11**, 431 (1990).
[61] M. Masino, A. Girlando, and Z. Soos, Chem. Phys. Lett. **369**, 428 (2003).
[62] A. Girlando, C. Pecile, and J. Torrance, Solid State Commun. **54**, 753 (1985).
[63] T. Salzillo, M. Masino, G. Kociok-Köhn, D. Di Nuzzo, E. Venuti, R. G. Della Valle, D. Vanossi, C. Fontanesi, A. Girlando, A. Brillante, and E. Da Como, Cryst. Growth Des. **16**, 3028 (2016).
[64] A. Girlando, Adv. Electron. Mater. **3**, 1600437 (2017).
[65] M. Yoshio and S. Gunzi, Bull. Chem. Soc. Jpn. **44**, 958 (1971).
[66] M. Masino, A. Girlando, L. Farina, and A. Brillante, Phys. Chem. Chem. Phys. **3**, 1904 (2001).
[67] M. Masino, A. Girlando, A. Brillante, R. G. D. Valle, and E. Venuti, Mater. Sci.-Poland **22**, 333 (2004).
[68] A. Fortunelli and A. Painelli, Phys. Rev. B **55**, 16088 (1997).